ZnO−Paper Based Photoconductive UV Sensor

3 AUTHORS, INCLUDING:

Alejandro J Gimenez

Universidad Autónoma de San Luis Potosí

12 PUBLICATIONS   **76** CITATIONS

SEE PROFILE

Jorge Seminario

Texas A&M University

232 PUBLICATIONS   **4,969** CITATIONS

SEE PROFILE

ZnO−Paper Based Photoconductive UV Sensor

Alejandro J. Gimenez,[†,‡] **J. M. Yáñez-Limón,**[‡] **and Jorge M. Seminario***[,†,§]

Department of Chemical Engineering and Department of Electrical and Computer Engineering, Texas A&M University, College Station, Texas, USA, and Centro de Investigación y Estudios Avanzados del Instituto, Politécnico Nacional Unidad Querétaro, Querétaro, México

Received: August 17, 2010; Revised Manuscript Received: November 14, 2010

We build sensors, capable of detecting and measuring ultraviolet (UV) light, by depositing zinc oxide (ZnO) powder from a solvent suspension over common white paper. Although these sensors are easy to fabricate and require inexpensive materials, they feature characteristics similar to those of UV sensors made with complex and expensive procedures. The good performance in terms of conductivity change of our simple devices can be attributed to the conductivity and porosity properties of paper, which effectively binds the ZnO crystals. We perform analyses using quantum chemistry methods to describe possible mechanisms that explain the conductivity changes observed on the ZnO surface due to doping interactions with interstitial hydrogen and doping depletion caused by oxygen adsorption.

1. Introduction

Light sensors usually go through a complex fabrication processes using expensive tools and materials. For the fabrication of a UV radiation (above 3.1 eV) sensor, ZnO is a good candidate because of its 3.3 eV band gap and large exciton energy of 60 meV.[1,2] The main drawback faced in the fabrication of UV sensors using ZnO comes from technical problems to dope ZnO with p carriers to create p−n junctions, thus limiting its use.[3] However, ZnO is not the only material used to sense UV light. Several methods have been developed to detect UV light; one common approach is using Si based sensors implementing filters to block the visible light spectrum, also wide band gap semiconductors such as AlGaN and diamond have been used with this purpose.[4,5] More recently, ZnO has been implemented as a photoconductive UV sensor in both macroscopically single crystal setups[6] as well as in nanostructured devices.[7−9]

In this work, we extend our work on sensors[10,11] by studying an extremely simple setup and evaluate its performance and potential for low cost applications. The sensor proposed in this work uses paper as a porous matrix to hold ZnO crystals; it has been proven that cellulose fibers effectively bind the ZnO without an additional binder, which could be useful for several technological applications.[12] This assembly forms a surface with ZnO crystals evenly distributed on top. When an electric field is applied to these ZnO crystals, a current is produced passing from one crystal to the other.

We use pencil-drawn graphite lines as electrodes on the paper. A typical 1 cm pencil line on paper has a resistance of about ∼10^4 Ω,[13] which is much lower compared with the ZnO paper devices studied in this work and that have a resistance in the order of ∼10^6−10^9 Ω. As a result, there is no need for low resistivity electrodes, facilitating the sensor fabrication.

ZnO is a naturally doped n-type semiconductor, and the reason for this doping is still under debate; it has been thought for a long time to be due to nonstoichiometry vacancies and crystal defects[14,15] and more recent studies claimed that the n-type doping is caused by unintentional hydrogen interstitial atoms embedded in the ZnO lattice.[16,17] In addition, it is well-known that chemical adsorption of atmospheric oxygen by ZnO depletes the charge carriers from the material surface in contact with air forming high resistance barriers, strongly decreasing the conductivity of ZnO crystals.[18−20]

Using density functional theory (DFT), we propose a mechanism to explain the origin of the natural doping of ZnO and the strong increase in superficial resistivity when oxygen from air is being adsorbed; these interactions may explain the sensitivity characteristics of photoconductive sensors implementing ZnO as the one we develop in the present work.

It has been proposed[21] that the reaction taking place on the ZnO surface involves adsorption of molecular oxygen from the atmosphere. Without the presence of UV light (under dark), adsorbed oxygen extracts free electrons from doped ZnO, creating electron depletion zones, and making the sensor less conductive.

$$O_2(g) + e^- \rightarrow O_2^-(ad) \tag{1}$$

$$O_2(g) + 2e^- \rightarrow O_2^{2-}(ad) \tag{2}$$
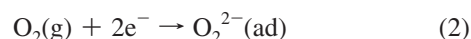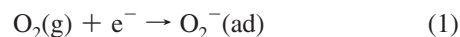
When the ZnO sensor is exposed to UV light, electron−hole pairs are generated. Holes will recombine with e^- adsorbed by oxygen ions and this action will release oxygen molecules back to air.

$$O_2^-(ad) + h^+ \rightarrow O_2(g) \tag{3}$$

$$O_2^{2-}(ad) + 2h^+ \rightarrow O_2(g) \tag{4}$$
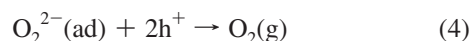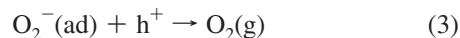
The electrons generated in this process contribute to increase the sensor conductivity.

[†] Department of Chemical Engineering, Texas A&M University.
[‡] Politécnico Nacional Unidad Querétaro.
[§] Department of Electrical and Computer Engineering, Texas A&M University.
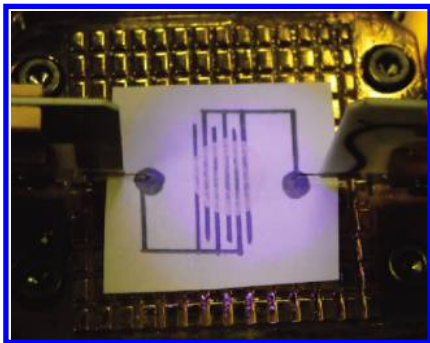
ZnO−Paper Based Photoconductive UV Sensor

J. Phys. Chem. C, Vol. 115, No. 1, 2011 **283**

Figure 1. Interdigitized sensor on a paper substrate connected to a probe station.

2. Methodology

We follow a theoretical-experimental approach to propose a mechanism that explains the resistivity changes observed in devices fabricated and tested in this work.

Experiment. We prepare a 10 mL water suspension with 0.1 g of ZnO powder (Sigma Aldrich ReagentPlus, powder, < 5 μm particle size, 99.9%); the powder is dispersed using an ultrasonic bath for 5 min and applied dropwise to several surfaces immediately before sonication to avoid precipitation and clustering. To observe the dye effect in the photocurrent, 50 mg of D-282, a stilbene based dye commonly used as a fluorescent whitening agent (FWA) in paper,[22] are added to the suspension. Then 0.1 mL drops are deposited onto glass and paper. Interdigitated graphite electrodes are drawn with a 4B pencil to achieve a large ZnO film area between electrodes as shown in Figure 1. To accelerate this process, a hot plate at 150 °C is used; water rapidly evaporates and leaves behind a homogeneous film of ZnO crystals.

The microscopic structure of the ZnO films as well as the one from the paper and the graphite electrodes have been studied using a FEI Quanta 600 FE-SEM microscope.[23] Electrical measurements of these films are made in a Desert Cryogenics TTP4 Cryogenic Probe Station using beryllium copper tips and a HP 4145A semiconductor analyzer. To test the photoconductivity of these films, we have used UV illumination from a 395 nm LED lamp at 10 cm from the film. The photoconductivity of these films and sensors is measured in two ways: (1) measuring the current with a bias voltage from 0 to 10 V to analyze the linearity of the device with and without UV illumination and (2) measuring the time evolution of current changes due to 0.1 Hz UV illumination signal to test the time response under a fix bias of 5 V. Wavelength response of the sensor device is measured using a 1000 W Xenon lamp Oriel model 66073 and a light monochromator Sciencetech 9050. Since the power distribution from the xenon lamp is not flat in the entire spectrum, it is required to normalize the measurements. This is achieved by measuring the lamp power with a Newport 1515-C Power meter.

Theory. To study electrical conductivity and optical characteristics of ZnO crystals, we perform ab initio calculations of very small clusters of ZnO (∼8 atoms) using the program Gaussian 03.[24] We are aware these results cannot be directly compared with those from our experiment or other ZnO studies because the particle size difference implies different properties;[25] however, these calculations provide a complementary knowledge on the electrical conductivity of ZnO.

We analyze five ZnO clusters, $\mathbf{a} = Zn_4O_4$, $\mathbf{b} = Zn_4O_3$, $\mathbf{c} = Zn_3O_4$, $\mathbf{d} = Zn_4O_4 + H$, and $\mathbf{e} = Zn_4O_4 + H + O$. $\mathbf{a}$ is found through a geometry optimization. $\mathbf{b}$−$\mathbf{e}$ are built by adding or

removing atoms from the optimized geometry of cluster $\mathbf{a}$. Single point calculations are performed to estimate electron energies. These single point calculations keep possible cluster structures that could be destroyed during an optimization; the results of this calculations yield information about the adjustments taking place when ZnO shows stoichiometric defects and interstitial hydrogen. The comparisons of clusters $\mathbf{b}$ and $\mathbf{c}$ are intended to analyze the effect of nonstoichiometry vacancies in ZnO. Cluster $\mathbf{d}$ yields information on the effect of interstitial hydrogen in the ZnO crystal, and cluster $\mathbf{e}$ is used to analyze the effect of oxygen adsorbed on the ZnO surface of an H doped crystal.

The electron energies and orbitals from the clusters are calculated with ab initio DFT.[24] We use the B3PW91 hybrid functional that combines the nonlocal Becke-3 (B3) exchange functional,[26] the generalized gradient approximation (GGA) of Perdew−Wang (PW91),[27] and an exchange component calculated similarly to Hartree−Fock (HF) but using the Kohn−Sham molecular orbitals instead. The basis set used in all these calculations is the 6-31G(d,p).[28,29] More precise calculations on the singlet and triplet dimer of Zn are performed using B3PW91/cc-pVTZ. The cc-pVTZ is a full electron basis set that uses a 7s,6p,4d,2f,1g basis for zinc[30] and 4s,3p,2d,1f for oxygen.[31] These methods have been widely tested in several types of systems from molecular electronics[32−39] to catalysis[40−42] to biological systems[43,44] and confirmed to provide acceptable results when compared to available experimental results; some of these methods yield results close to chemical accuracy[45−52]

3. Results and Discussion

The current−voltage behavior of the simple ZnO−paper devices is characterized experimentally by performing electrical measurements under UV light. The energy response is measured by applying light of different wavelengths from visible to ultraviolet while measuring the conductivity of the device under a fix bias. Besides these experimental studies, we perform ab initio calculations, which help us understand the strong conductivity changes in ZnO photoconductive devices.

Experiment. From the FE-SEM microscopy characterization of our sensor devices we observe that paper, as is well-known, is formed by cellulose fibers. The space between fibers makes a microscopically rough surface that helps to hold the ZnO crystals (Figure 2). In this study we also confirm that the pencil lines are formed by graphite layers spread over the paper; the detail of these layers is shown in Figure 2b. On the other hand, the ZnO crystals on paper form a film of ZnO composed of agglomerated crystals forming a relatively uniform layer, which is compact enough to conduct a measurable electrical current, as can be identified in Figure 2c. These crystals have a uniform size distribution of approximately a few hundred of nanometers, as shown in the agglomerated crystals (Figure 2d).

The substrate current measured (Figure 3) in bare glass is on the order of 10^{-13} A; this represents a much higher resistance from glass compared with the one of bare paper, which allows currents on the order of 10^{-9} A, about 4 orders of magnitude higher. ZnO films on both surfaces show a photocurrent effect when illuminated by UV light. It is worth noticing that the photoconductivity in paper is more linear compared to the one of glass, and the resistance of ZnO films over paper has characteristics similar to those of the substrate without ZnO. Measuring tips where placed 1 mm apart.

The UV response with time of ZnO films over glass and paper is shown in Figure 4. This measurements are done while applying UV light pulses to the photoconductive films for 10 s.
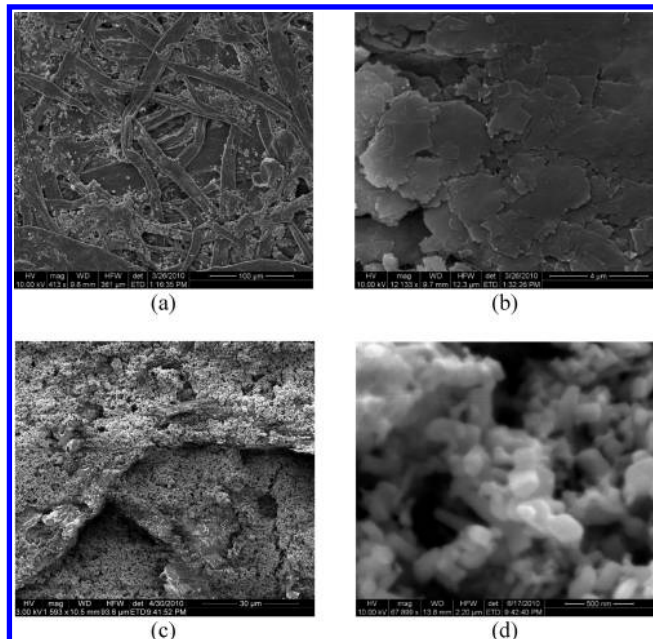
Figure 2. FE-SEM images of (a) paper substrate, (b) graphite lines, (c) ZnO crystals on paper, and (d) ZnO crystals on paper.
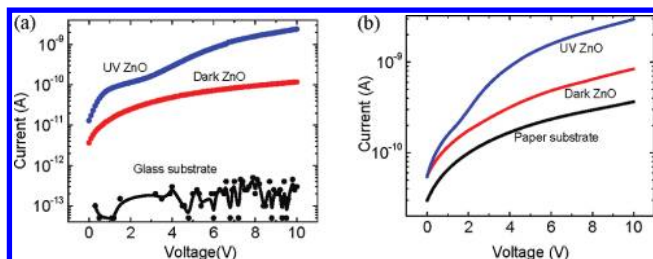

Figure 3. (a) $I-V$ characteristic of ZnO films on glass and (b) $I-V$ characteristics of ZnO films on paper. ZnO film under UV illumination (blue). ZnO film on dark (red) and substrate without ZnO (black).
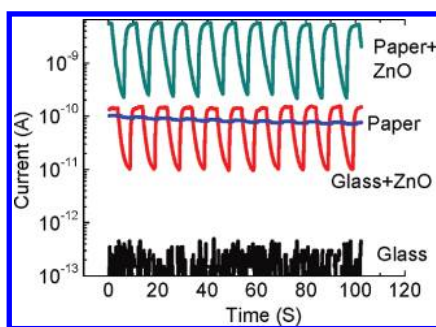

Figure 4. Time dependent response of ZnO films on glass and paper while applying 0.1 Hz UV light pulses.

There is a large difference between the current passing through the glass substrate and the paper substrate (Figure 4). There exists a small photocurrent effect in the bare paper that could imply that some of the components included in paper are photosensitive. The ZnO film on paper substrate yields a photocurrent effect about 10 times larger compared to the photocurrent effect shown on glass.

Current versus voltage ($I-V$) measurements are performed on a sensor device before adding ZnO having only paper with graphite electrodes drawn. The current measured from this device under dark is o the order of 10^{-9} A; when UV light is shone on this device, its current increases slightly. Plots of device measurements without ZnO are shown in Figure 5. As the $I-V$ curves for the device under dark and under UV are
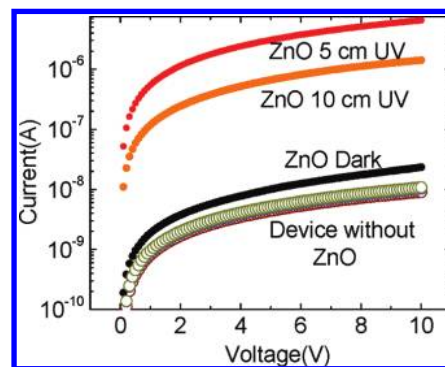

Figure 5. Current versus voltage measurements of a sensor device with and without ZnO. The behavior of the sensor device with ZnO (solid lines) is shown under dark conditions and under UV at 5 and 10 cm from the sample. The effect of UV light on a device without ZnO (circles) is too small to be appreciated in the plot.
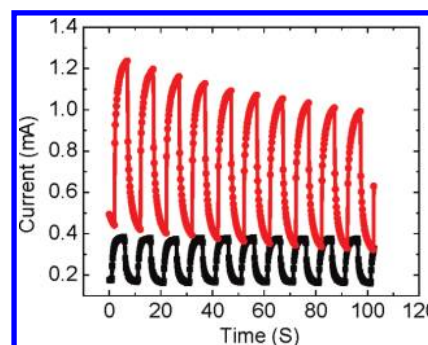

Figure 6. Time dependent response of UV sensors with (red) and without (black) dye while applying 0.1 Hz UV light pulses.

very similar, they practically overlap in the logarithmic plot. The same device is tested after adding ZnO;the current of this device at dark is o the order of 10^{-8} A. When a ZnO–paper device is exposed to a UV light source at a distance of 10 cm, there is an increment of roughly 60 times the current measured under dark conditions. When the light source is at 5 cm from the sensor, the current increment goes as high as 280 times more than the current at dark (Figure 5). The ratio of the current values from these measurements is 4.6, which is close to the expected value 4 from the inverse-square law.

To evaluate the interaction of FWA dyes and the photocurrent behavior of ZnO crystals, we test two sensors similar to the one depicted in Figure 1; one sensor has FWA dye and the other does not. The behavior comparison (Figure 6) shows that the sensor with dye yields a higher photocurrent than the one without dye. However, this effect has a strong time ependence and fades with time; this fading could be probably attributed to dye degradation. The photoconductivity of a ZnO–paper device without dye shows a steadier behavior, which is a desirable property of a sensor device.

From the wavelength response analysis we know that the sensor device becomes sensitive at ~410 nm with a small peak at 380 nm and a larger one at 340 nm (Figure 7). These peaks are probably due to the electron bands of ZnO. At approximately 250 nm, sensitivity decreases to nearly zero.

Theory. A Zn_4O_4 singlet cluster of spin zero has been optimized yielding an irregular cube with approximately 1.96 Å per side and another of high spin, $s = 4$ yields 2.09 Å. Table 1 compares calculated parameters with experimental data of ZnO bulk material. The Zn_4O_4 cluster bond lengths for the low spin are generally shorter compared with the data from the ZnO bulk crystal. As this is a small cluster, it is expected that the atoms
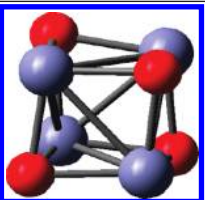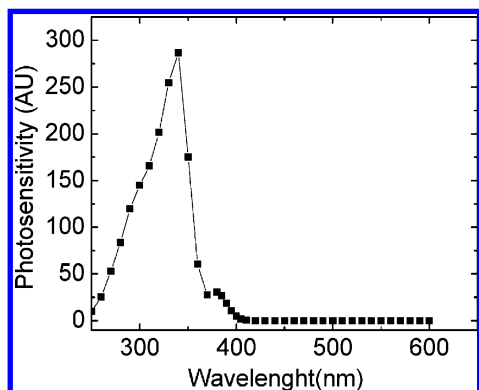
ZnO−Paper Based Photoconductive UV Sensor

J. Phys. Chem. C, Vol. 115, No. 1, 2011 **285**

Figure 7. Sensor photosensitivity intensity versus wavelength.

TABLE 1: Average Bond Distances (Å) and HLG versus Bandgap (eV) Comparisons of Theory and Experiment Results[a]

	theory $(s = 0)$	theory $(s = 4)$	experiment1
d_{Zn-Zn}	2.61	3.35	3.25
d_{Zn-O}	1.96	2.09	1.99
d_{O-O}	2.99	3.19	3.25
gap	3.59	3.39	3.37

[a] Theoretical calculations of a singlet (low spin) and nonet (high spin) of a Zn_4O_4 cluster optimized by ab initio theory versus bulk ZnO experimental measurements.[1] Low spin results show a sharp contrast with experimental geometry; however increasing the spin of the cell also increases the matching to the experimental geometry. The Zn−Zn distances for $s = 0, 1, 2, 3, 4$ are 2.61, 2.73, 2.66, 3.10, and 3.35 Å, respectively. The best matching to the experimental geometry is when all atoms have a radical electron, $s = 4$. The gap for the high spin is the average of α and β gaps.

form shorter bonds because the lack of other neighbors interactions available in a large crystal. A calculation of the singlet Zn dimer yields a distance of 3.33 Å, which is more compatible with the experimental value found for the bulk; however, the triplet structure (51.3 kcal/mol above the singlet) yields a bond length of 2.38 Å. Thus it is not surprising to have such a variety of bond distances for Zn. The large amount of
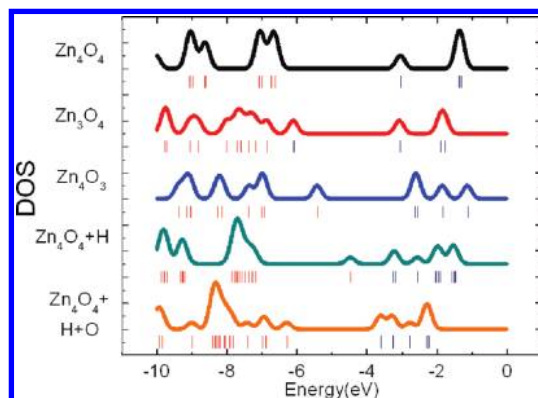

Figure 9. Zn_4O_4 (HLG = 3.59 eV), Zn_3O_4 (HLG = 0.76 eV), Zn_4O_3 (HLG = 2.79 eV), $Zn_4O_4 + H$ (HLG = 1.22 eV), and $Zn_4O_4 + H + O$ (HLG = 2.67 eV) clusters DOS. Below each DOS, vertical bars represent orbital energy levels (red bars are occupied states and blue bars are unoccupied states).

dangling bonds in the smaller cluster is compensated by bringing closer all atoms in the cluster than they are in the bulk. Also, the predicted highest occupied molecular orbital (HOMO)−lowest unoccupied molecular orbital (LUMO) gap (HLG) for the singlet ($s = 0$) cluster is 3.59 eV, which is not too far from the experimental band gap value of 3.37 eV of bulk ZnO. Table 1 also shows the results for the high spin cluster ($s = 4$).

Departing from the optimized Zn_4O_4 cluster, we have applied modifications and made single point calculations to compare a few cases Zn_4O_3, Zn_3O_4, $Zn_4O_4 + H$, and $Zn_4O_4 + H + O$. Figure 8 depicts the geometry, highest occupied molecular orbital (HOMO), and lowest unoccupied molecular orbital (LUMO) of the studied cases. These visualizations aid us in understanding trends of the electrical conductivity of the ZnO cluster under several situations. It is important to notice that for the cases Zn_4O_3 and $Zn_4O_4 + H$, there is a large delocalized evenly distributed HOMO orbital. This implies that in both cases, oxygen vacancies and interstitial H may help to improve the electrical conductivity of ZnO. Besides, we can observe that when there is an extra oxygen atom such as in the case of $Zn_4O_4 + H + O$, the HOMO strongly localizes around the extra oxygen atom, making the cluster less electrically conductive.

The density of state (DOS) of the clusters yields useful information to study their semiconductor properties. In Figure 9,
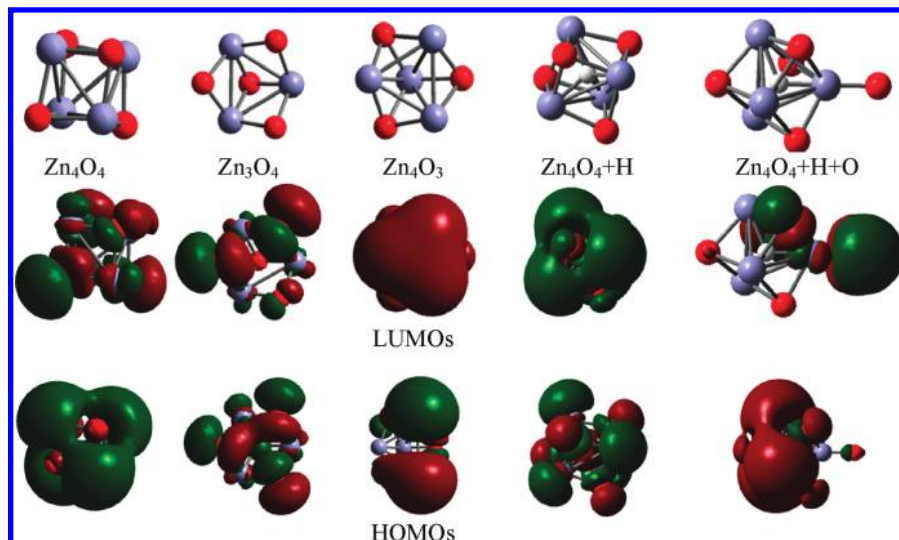

Figure 8. Geometries LUMOs and HOMOs for Zn_4O_4, Zn_3O_4, Zn_4O_3, $Zn_4O_4 + H$, and $Zn_4O_4 + H + O$.

the clusters DOS can be compared. From the Zn_4O_4 DOS, a large band gap of 3.59 eV is calculated, in good agreement with the well-known ZnO band gap value of 3.37 eV. For Zn_3O_4, we calculate a small band gap of 0.76 eV, which comes from an orbital change induced by a Zn vacancy of the cluster. The energy proximity of this orbital with the HOMO band may be regarded as a p-type doping level. On the other hand, the DOS for Zn_4O_3 and Zn_4O_4 + H have a higher HOMO energy when compared with the base cluster Zn_4O_4. These higher energy levels could be regarded as n-type doping levels caused by O vacancies and interstitial H, especially the case having interstitial H because the doping energy level is closer to the LUMO. In the case of Zn_4O_4 + H + O, the HOMO lowers its energy to a level close to the HOMO in the Zn_4O_4. It can be inferred that oxygen takes the electron from the doping produced by the interstitial H and creates a depletion zone rendering the cluster less conductive.

4. Conclusions

We develop a method to design very low cost and easy to fabricate UV sensors. Performance tests show that ZnO films from a water−ZnO powder suspension on paper feature photocurrent properties strong enough to be used in UV sensing applications. Measurements comparing properties of ZnO films on paper and glass show better performance than measurements on paper substrates. Thus, much larger photocurrents are obtained on paper substrates. We believe there are several reasons involved in making paper a good substrate; the most relevant is that paper resistivity is slightly higher compared to ZnO powder film resistivity. This similarity in resistances between ZnO and paper could imply that electric current preferentially flows on the ZnO film; however, in the points where there are cracks on the ZnO film, some current is still allowed to flow through the substrate, explaining the better linearity and higher photocurrent achieved on paper substrates. Another reason involved in the better performance of paper is the porosity, which could give better attachment of ZnO micro- and nanoparticles to the substrate. We also notice that an increment in the FWA dye results in a larger photocurrent from the sensors; however, this enhancement in photocurrent seems to decay as the dye degrades and it is not yet identified if the dye is absorbing light and transferring charge carriers to the ZnO or if it is only working as a low resistance binder between ZnO particles.

Despite being extremely easy to fabricate, the ZnO−paper UV sensor performance is comparable to other kinds of UV sensors. For instance, the spectral sensitivity of the ZnO−paper sensor shows a better selectivity to UV compared with Si UV sensing devices.[53] The sensitivity of the device developed in this work in terms of UV current as a ratio of dark current is in the range of 2 orders of magnitude, which is similar to the one observed on other nanostructured ZnO sensor devices.[7,8,21]

Ab initio analysis in this work corroborates that the strong changes in resistance of the developed sensor are mainly due to the process of adsorption and desorption of oxygen; the adsorption of oxygen at the surface of ZnO crystals localizes doping carriers, creating a depletion zone at the surface of the crystal. As the structure of these sensors is mainly composed of nano- and microsized crystals conducting an electrical current, the change of resistance of the sensor is enhanced and allows creating sensitive sensors in a simple way.

References and Notes

(1) Ozgur, U.; et al. A comprehensive review of ZnO materials and devices. *J. Appl. Phys.* **2005**, *98*, 041301−103.

(2) Chen, Y.; et al. ZnO as a novel photonic material for the UV region. *Mater. Sci. Eng. B* **2000**, *75*, 190–198.

(3) Look, D. C.; Claflin, B. P-type doping and devices based on ZnO. *Phys. Status Solidi B* **2004**, *241*, 624–630.

(4) Razeghi, M.; Rogalski, A. Semiconductor ultraviolet detectors. In *Photodetectors: Materials and Devices*; SPIE: San Jose, CA, U.S., 1996; pp 114−125.

(5) Binari, S. C.; et al. Diamond metal-semiconductor-metal ultraviolet photodetectors. *Diamond Relat. Mater.* **1993**, *2*, 1020–1023.

(6) Masuoka, F.; et al. Applicability of ZnO single crystals for ultraviolet sensors. *Physica Status Solidi C* **2006**, *3*, 1238–1241.

(7) Hullavarad, S.; et al. Ultra violet sensors based on nanostructured ZnO spheres in network of nanowires: a novel approach. *Nanoscale Res. Lett.* **2007**, *2*, 161–167.

(8) Hullavarad, S.; et al. Persistent Photoconductivity Studies in Nanostructured ZnO UV Sensors. *Nanoscale Res. Lett.* **2009**, *4*, 1421–1427.

(9) Soci, C.; et al. ZnO Nanowire UV Photodetectors with High Internal Gain. *Nano Lett.* **2007**, *7*, 1003–1009.

(10) Rangel, N. L.; et al. Light-Activated Molecular Conductivity in the Photoreactions of Vitamin D3. *J. Phys. Chem. A* **2009**, *113*, 6740–6744.

(11) Gimenez, A. J.; et al. Analysis of Nano and Molecular Arrays of Negative Differential Resistance Devices for Sensing and Electronics. *IEEE Sens. J.* **2009**, *9*, 1136–1141.

(12) Ghule, K.; et al. Preparation and characterization of ZnO nano-particles coated paper and its antibacterial activity study. *Green Chem.* **2006**, *8*, 1034–1041.

(13) Woolf, L. D.; Streckert, H. H. Graphite pencil line for exploring resistance. *Phys. Teach.* **1996**, *34*, 440–441.

(14) Schmidt-Mende, L.; MacManus-Driscoll, J. L. ZnO - nanostructures, defects, and devices. *Mater. Today* **2007**, *10*, 40–48.

(15) Zhang, S. B.; et al. Intrinsic n-type versus p-type doping asymmetry and the defect physics of ZnO. *Phys. Rev. B* **2001**, *63*, p. 075205.

(16) Van de Walle, C. G. Hydrogen as a Cause of Doping in Zinc Oxide. *Phys. Rev. Lett.* **2000**, *85*, p. 1012.

(17) Janotti, A.; Van de Walle, C. G. Hydrogen multicentre bonds. *Nat. Mater.* **2007**, *6*, 44–47.

(18) Li, Q. H.; et al. Adsorption and desorption of oxygen probed from ZnO nanowire films by photocurrent measurements. *Appl. Phys. Lett.* **2005**, *86*, 123117–3.

(19) Melnick, D. A. Zinc Oxide Photoconduction, an Oxygen Adsorption Process. *J. Chem. Phys.* **1957**, *26*, 1136–1146.

(20) Shao-Pin, C.; et al. Electrical conduction mechanisms in natively doped ZnO nanowires. *Nanotechnology* **2009**, *20*, p. 015203.

(21) Chai, G.; et al. Crossed zinc oxide nanorods for ultraviolet radiation detection. *Sens. Actuators, A* **2009**, *150*, 184–187.

(22) Roberts, J. C. *Paper chemistry*, 2nd ed.: Springer: Berlin, 1996.

(23) Goldstein, D. E. N. Joseph; Joy, David C.; Echlin, Patrick; Lyman, Charles E.; Lifshin, Eric. *Scanning electron microscopy and x-ray microanalysis*, 3rd ed.: Springer: Berlin, 2003.

(24) Frisch, M. J.; et al. *Gaussian-2003*, Revision D.2; Gaussian, Inc.: Pittsburgh, PA, U.S., 2003.

(25) Bahnemann, D. W.; et al. Preparation and characterization of quantum size zinc oxide: a detailed spectroscopic study. *J. Phys. Chem.* **1987**, *91*, 3789–3798.

(26) Becke, A. D. Density-functional thermochemistry. IV. A new dynamical correlation functional and implications for exact-exchange mixing. *J. Chem. Phys.* **1996**, *104*, 1040–1046.

(27) Perdew, J. P. Unified Theory of Exchange and Correlation beyond the Local Density Approximation. In *Electronic Structure of Solids*; Ziesche, P., Eschrig, H., Eds.; Akademie Verlag: Berlin, 1991; pp 11−20.

(28) Becke, A. D. Density-functional thermochemistry III. The role of exact exchange. *J. Chem. Phys.* **1993**, *98*, 5648–5652.

(29) Hohenberg, P.; Kohn, W. Inhomogeneous electron gas. *Phys. Rev. B* **1964**, *136*, 864–871.

(30) Balabanov, N. B.; Peterson, K. A. Systematically convergent basis sets for transition metals. I. All-electron correlation consistent basis sets for the 3d elements Sc--Zn. *J. Chem. Phys.* **2005**, *123*, 064107–15.

ZnO−Paper Based Photoconductive UV Sensor

J. Phys. Chem. C, Vol. 115, No. 1, 2011 **287**

(31) Dunning, T. H., Jr. Gaussian basis sets for use in correlated molecular calculations. I. The atoms boron through neon and hydrogen. *J. Chem. Phys.* **1989**, *90*, 1007–1030.

(32) Rangel, N. L.; Seminario, J. M. Molecular Electrostatic Potential Devices on Graphite and Silicon Surfaces. *J. Phys. Chem. A* **2006**, *110*, 12298–12302.

(33) Yan, L.; et al. Terahertz Signal Transmission in Molecular Systems. *Int. J. High Speed Electron. Syst.* **2006**, *16*, 669–675.

(34) Yan, L.; et al. Encoding Information Using Molecular Vibronics. *J. Nanosci. Nanotechnol.* **2006**, *6*, 675–684.

(35) Seminario, J. M., et al. Nano-Detectors Using Molecular Circuits Operating at THz Frequencies. *Proc. SPIE 5995*, **2005**; 59950R-1 to 59950R-15.

(36) Seminario, J. M.; et al. Transmission of Vibronic Signals in Molecular Circuits. *J. Phys. Chem. A* **2005**, *109*, 9712–9715.

(37) Seminario, J. M.; et al. Scenarios for Molecular-Level Signal Processing. *Proc. IEEE* **2005**, *93*, 1753–1764.

(38) Seminario, J. M.; et al. Encoding and transport of information in molecular and biomolecular systems. *Proceedings of the 2005 5th IEEE Conference on Nanotechnoly* **2005**, *1*, 65–68.

(39) Seminario, J. M.; Yan, L. Cascade configuration of logical gates processing information encoded in molecular potentials. *Int. J. Quantum Chem.* **2007**, *107*, 754–761.

(40) Wang, K.; et al. Switchable Molecular Conductivity. *J. Am. Chem. Soc.* **2009**, *131*, 10447–10451.

(41) Sotelo, J. C.; Seminario, J. M. Local reactivity of O_2 with Pt_3 on Co_3Pt and related backgrounds. *J. Chem. Phys.* **2008**, *128*, 204701(1−11).

(42) Sotelo, J. C.; Seminario, J. M. Biatomic substrates for bulk-molecule interfaces: The PtCo-oxygen interface. *J. Chem. Phys.* **2007**, *127*, 244706(1−13).

(43) Salazar-Salinas, K.; Seminario, K. M. Energetics and Vibronics Analyses of the Enzymatic Coupled Electron-Proton Transfer from NfsA Nitroreductase to Trinitrotoluene. *IEEE Nano. Trans.*, submitted for publication.

(44) Salazar, P. F.; Seminario, J. M. Identifying Receptor-Ligand Interactions through an ab Initio Approach. *J. Phys. Chem. B* **2008**, *112*, 1290–1292.

(45) Salazar, P. F.; Seminario, J. M. Simple Energy Corrections for Precise Atomization Energies of CHON Molecules. *J. Phys. Chem. A* **2007**, *111*, 11160–11165.

(46) Jauregui, L. A.; et al. Transverse Electronic Transport in Double-Stranded DNA Nucleotides. *J. Phys. Chem. B* **2009**, *113*, 6230–6239.

(47) Politzer, P.; Seminario, J. M. Energy Changes Associated with Some Decomposition Steps of 1,3,3-Trinitroazetidine - a Nonlocal Density-Functional Study. *Chem. Phys. Lett.* **1993**, *207*, 27–30.

(48) Politzer, P.; et al. A Proposed Interpretation of the Destabilizing Effect of Hydroxyl-Groups on Nitroaromatic Molecules. *Chem. Phys. Lett.* **1989**, *158*, 463–469.

(49) Seminario, J. M.; et al. A Density Functional/Molecular Dynamics of the Structure of Liquid Nitromethane. *J. Chem. Phys.* **1995**, *102*, 8281–8282.

(50) Seminario, J. M.; et al. Calculated Structures and Relative Stabilities of Furoxan, some 1,2 Dinitrosoethylenes and other Isomers. *J. Comput. Chem.* **1992**, *13*, 177–182.

(51) Politzer, P.; Seminario, J. M. Computational study of the structure of dinitraminic acid, $HN(NO_2)_2$ and the energetics of some possible decomposition steps. *Chem. Phys. Lett.* **1993**, *216*, 348–352.

(52) Derosa, P. A.; et al. Properties of Small Bimetallic Ni-Cu Clusters. *J. Phys. Chem. A* **2001**, *105*, 7917–7925.

(53) Yamada, H.; et al. A UV Sensor IC based on SOI Technology for UV care applications. Presented at the SICE Annual conference, 2008, University Electro-Communications: Tokyo, Japan, 2008.